Effect of temperature and compositional changes on the phonon properties of Ni-Mn-Ga shape memory alloys

Semih Ener,[*] Jürgen Neuhaus,[†] and Winfried Petry[†]
Lehrstuhl für Funktionelle Materialien, Physik Department, Technische Universität München, D-85747 Garching, Germany

Richard Mole and Klaudia Hradil[‡]
Forschungs-Neutronenquelle Heinz Maier-Leibnitz (FRM II), Technische Universität München, D-85747 Garching, Germany

Mario Siewert, Markus E. Gruner, and Peter Entel
Faculty of Physics and Center for Nanointegration, CeNIDE, University of Duisburg-Essen, D-47048 Duisburg, Germany

Ivan Titov and Mehmet Acet
Fachbereich Physik, Experimentalphysik, Universität Duisburg-Essen, D-47048 Duisburg, Germany
(Received 4 June 2012; revised manuscript received 31 July 2012; published 11 October 2012)

We report on the vibrational properties of the ferromagnetic shape memory alloy system Ni-Mn-Ga in its stoichiometric Ni_2MnGa and off-stoichiometric $Ni_{49}Mn_{32}Ga_{19}$ compositions. Elastic and inelastic neutron scattering measurements at different temperatures are presented with a focus on the austenite phase and compared to first-principles calculations. The overall behavior of the full phonon dispersion is similar for both compositions with remarkable exceptions for the $TA_2[\xi\xi 0]$ acoustic branch and optical phonon branches. Less dispersion is found in the optical phonons for $Ni_{49}Mn_{32}Ga_{19}$ in the whole reciprocal space when compared to Ni_2MnGa and is explained by the occupation of regular Ga sites by excess Mn atoms. A pronounced softening in the $TA_2[\xi\xi 0]$ phonon branch within the austenite phase is observed in both samples when approaching the martensitic transition. Its location in reciprocal space reveals the martensitic transition mechanism. The austenite $L2_1$ structure transforms to the tetragonal modulated martensite structure by shuffling (110) planes in the $[1\bar{1}0]$ direction, similarly to what has been observed at the martensitic transitions of the d^1 and d^2 transition metals. Whereas the temperature dependence of the softening of the $TA_2[\xi\xi 0]$ phonons in the stoichiometric sample coincides perfectly with the magnetic and structural transitions, this is not the case for the off-stoichiometric sample. Here the relation between the magnetic ordering and the vibrational properties is still an open question.

DOI: 10.1103/PhysRevB.86.144305 PACS number(s): 63.20.−e, 81.30.Kf

I. INTRODUCTION

Materials which are able to recover a stress-induced deformation by passing through a structural transition temperature are known as shape memory materials. The high-symmetry, high-temperature phases of these kinds of materials are called austenite, whereas the low-symmetry, low-temperature phases are called martensite.[1] In particular, magnetic shape memory alloys are attractive for smart material applications like actuators or sensors due to their unique properties, such as, for example, magnetic-field-induced structural transition and magnetic-field-induced variant reorientation.

Ni-Mn-Ga alloys are the most widely investigated materials for magnetic shape memory applications using a large variety of different methods.[2–9] The important property of the Ni-Mn-*X* system is the tunability of their structural transition and magnetic ordering temperatures by changes in the chemical composition, i.e., changes in the number of valence electrons per atom.[9,10] The amount of the deformation in the shape memory effect is strongly related to the crystallographic structure of the low-temperature martensite phase. For off-stoichiometric Ni-Mn-Ga alloys 10% and 6% of elongations are observed for the seven-layered and five-layered martensite phases, respectively.[11,12]

For the Ni-Mn-Ga system the high-temperature austenite phase is the $L2_1$ face-centered cubic (fcc) structure (space group $Fm3m$). The martensite and premartensite transformations are driven by pronounced phonon softening in the $TA_2[\xi\xi 0]$ branch of the austenite phase.[13–17] In an early first-principles-based approach, Enkovaara *et al*. reproduced the temperature-dependent $L2_1$-$L1_0$ transformation semiquantitatively taking advantage of the Debye approximation.[18] The correct thermal sequence of phases, taking into account the threefold-modulated premartensitic structure, is achieved only by including vibrational and magnetic contributions to the free energy as first shown by Uijttewaal *et al*.[19] Siewert *et al*.[20] demonstrated by calculating the free-energy contributions along the $L2_1$-$L1_0$ transformation path that indeed both vibrational entropy and magnetic excitations also determine the first-order transition between the nonmodulated martensite and the austenite. The $TA_2[\xi\xi 0]$ branch corresponds to a phonon propagation in the (110) direction with transverse $[1\bar{1}0]$ elongation. Selective phonon investigations for Ni-Mn-Ga alloys have been reported in the literature[13–17] but a detailed investigation of the temperature- and composition-dependent dynamics is missing. The off-stoichiometric Mn-rich alloy allows one to investigate an increasing antiferromagnetic interaction. Furthermore, this composition is used for technical applications in the low-temperature five-layered martensite phase.

This paper reports on measurements of composition- and temperature-dependent vibrational properties of Ni-Mn-Ga alloys and compares these results with first-principles

calculations. We focus here on the complete phonon dispersions of stoichiometric and off-stoichiometric compositions in the austenite phase and the effect of temperature on the phonon softening along the $TA_2[\xi\xi 0]$ phonon branch in the austenite and martensite phases.

II. SAMPLE CHARACTERIZATION

The Ni-Mn-Ga single crystals were grown by R. Schneider and K. Rolfs at the Helmholtz-Zentrum Berlin (HZB) using the slag remelting and encapsulation (SLARE) technique.[21] As unavoidable for Bridgman-grown crystals, small compositional gradients occur along the crystal growth direction. For both crystals compositional gradients along the growth direction of max. 1% have been determined. At room temperature the stoichiometric (Ni_2MnGa) sample has an $L2_1$ Heusler structure with the unit-cell constant of 5.84 Å. Above 350 K the off-stoichiometric $Ni_{49}Mn_{32}Ga_{19}$ alloy exhibits the same structure with the unit-cell constant of 5.82 Å. Neutron diffraction on the single-crystal diffractometer RESI (Ref. 22) at the Forschungs-Neutronenquelle Heinz Maier-Leibnitz (FRM II) shows the expected ordering of the Heusler structure. The Ni positions are occupied by only the Ni atoms, the Mn sites are entirely occupied by Mn atoms, and the remaining Ga site is partly filled at 20.7% with the excess of Mn atoms.

To extend the temperature range of the phonon measurement, single variant crystals of the off-stoichiometric composition were prepared by mechanical training on cooling the austenitic sample through the phase transition temperature under uniaxial pressure along a crystallographic axis.[21]

The actual compositions of the samples were determined by energy-dispersive x-ray spectroscopy to be $Ni_{50}Mn_{26}Ga_{24}$ for the stoichiometric composition and $Ni_{49}Mn_{32}Ga_{19}$ for the off-stoichiometric composition. The compositional gradients along the samples are smaller than 1% for both samples.

In order to characterize the magnetic and structural phase transitions, temperature-dependent magnetization $M(T)$ and differential scanning calorimetry (DSC) measurements were carried out. For the magnetization measurements a superconducting quantum interference device (SQUID) magnetometer was used. $M(T)$ data were obtained in zero-field cooled (ZFC), field-cooled (FC), and field-heated (FH) modes in a temperature interval of $7 \leqslant T \leqslant 380$ K and under a magnetic field of 5 mT. The structural transition temperatures and the Curie temperature are defined from these magnetization measurements.

Figure 1(a) shows the temperature-dependent magnetization measurements of stoichiometric Ni_2MnGa. M_S, M_F, A_S, A_F, and T_C correspond to the martensite start, martensite finish, austenite start, austenite finish, and Curie temperatures, respectively. The austenite to premartensite transition start temperature ($M_S^{A\text{-}3M}$), premartensite to martensite transition start temperature ($M_S^{3M\text{-}M}$), and the corresponding transition finish temperatures ($M_F^{A\text{-}3M}$ and $M_F^{3M\text{-}M}$) are defined by the temperature derivative of the FC measurement. The reverse transition temperatures are defined accordingly by the FH measurement. The obtained temperatures are given in the inset of Fig. 1(a). $A_S^{3M\text{-}A}$ could not be observed due to the overlapping of this temperature with $A_F^{M\text{-}3M}$. The martensite transition temperatures are in a perfect agreement with the diffraction measurements [Fig. 8(a)]. The Curie temperature of Ni_2MnGa is not observed in the magnetization measurements for temperatures up to 380 K. For this sample a DSC measurement shows $T_C = 383.0$ K, in accordance with Ref. 23. In the martensite phase there is a deviation between the ZFC and FC measurements of Ni_2MnGa which can be explained by the antiferromagnetic Mn-Mn interactions caused by the small deviation from stoichiometry.

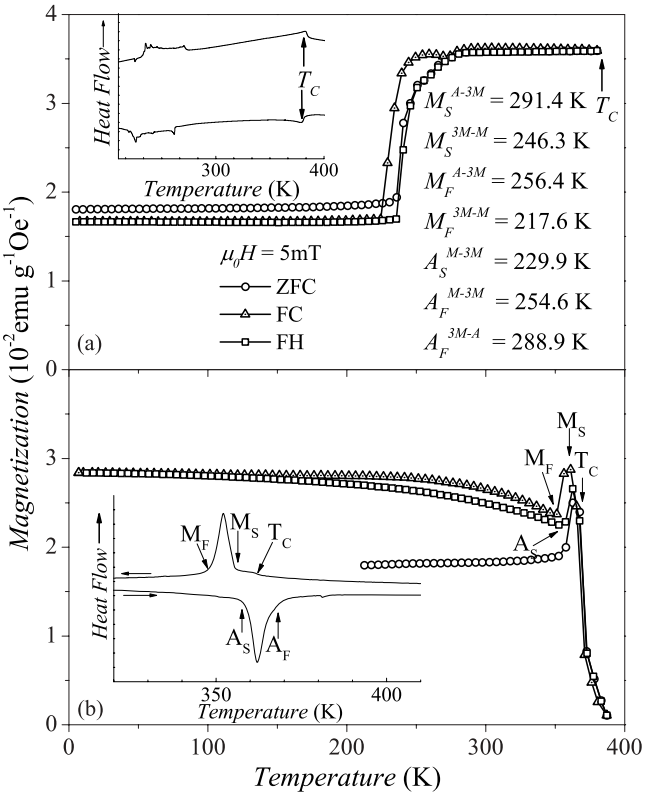

FIG. 1. Magnetization of (a) Ni_2MnGa and (b) $Ni_{49}Mn_{32}Ga_{19}$ as a function of temperature. ZFC indicates the zero-field-cooled, FC, the field-cooled, and FH the field-heated measurements. The insets show the corresponding DSC measurements.

The $M(T)$ measurements of $Ni_{49}Mn_{32}Ga_{19}$ are shown in Fig. 1(b) together with corresponding DSC data (inset). The obtained transition temperatures of $M_S = 361.1$ K, $M_F = 351.2$ K, $A_S = 357.5$ K, $A_F = 362.5$ K, and $T_C = 371.2$ K agree for both measurements.

The $M(T)$ measurements show that $Ni_{49}Mn_{32}Ga_{19}$ is paramagnetic for temperatures above 371.2 K. The difference between the ZFC and the FC measurements indicates the presence of antiferromagnetic interactions in $Ni_{49}Mn_{32}Ga_{19}$ which can be attributed to the excess of Mn in the sample. 20.7% of the Mn atoms occupy the Ga sites and the distance between these Mn atoms and the Mn atoms on the original Mn sites becomes small enough to create antiferromagnetic Mn-Mn interactions. Similar behavior of the antiferromagnetic ordering has been observed and calculated for Ni-Mn-X materials.[24,25] Accordingly, the Mn-Mn interactions in ordered stoichiometric Ni_2MnGa are ferromagnetic.

III. INELASTIC NEUTRON SCATTERING SETUP

The phonon measurements were taken at the three-axis spectrometer PUMA using thermal neutrons from the FRM II in Garching, Germany. For temperatures below 300 K, the measurements were taken with the sample mounted in an aluminum container placed in a helium closed-cycle cryostat. The aluminum container was filled with inert gas to ensure a good thermal contact. The high-temperature measurements were performed in a vacuum furnace with the samples mounted on a niobium sample holder. Temperature control and stability using the cryostat were better than 0.1 K. For the furnace we reached a stability better than 0.5 K.

The phonon measurements have been performed in constant-k_f mode using the PG(002) analyzer. To ensure a low scattering background a sapphire filter was placed in front of the PG(002) monochromator to suppress fast neutrons. A graphite filter in front of the analyzer was used to diminish higher-order scattering. The scans have been performed mainly in constant-**q** mode. Constant-ω scans were used at points in the phonon dispersion whenever the resolution ellipsoid of the instrument gave favorable results for this setup.

To achieve an optimum of energy resolution and neutron flux, vertical as well as horizontal focusing was used at both the monochromator and the analyzer especially for the high-energy optical modes. Even for the dispersive acoustic modes no additional collimation was needed. Special care was taken to optimize the setup for low scattering background using the numerous slit systems at the instrument. The primary slit acting as virtual neutron source was tuned to match the respective sample size.

IV. COMPUTATIONAL DETAILS

The measured phonon dispersion is compared to results of *ab initio* calculations using the methods of density functional theory. The theoretical phonon dispersion was generated by means of the direct approach,[26–28] calculating the Hellmann-Feynman forces using the Vienna *ab initio* simulation package[29,30] (VASP) together with the projector augmented wave method.[31] The generalized gradient approximation in the formulation of Perdew, Burke, and Ernzerhof[32] was used as the exchange-correlation functional. The energy cutoff was chosen to be 450 eV.

Displacement sizes of 0.02 Å, a k-point grid of $2 \times 2 \times 2k$ points for the $L2_1$-structure, and Methfessel-Paxton smearing with a smearing parameter $\sigma = 0.1$ eV were applied.[33] The supercell was generated by repeating the primitive cell four times in each direction, resulting in a cell size of 256 atoms, allowing the accurate calculation of phonon dispersions along all directions in the Brillouin zone as well as the calculation of the vibrational density of states (DOS). The interatomic force constants and dynamical matrices were obtained using the PHON code of Alfé.[34] The DOS was generated using a mesh consisting of $61 \times 61 \times 61$ q points.

In our extensive calculations we placed special emphasis on the elemental character of the respective phonon modes. It turns out that the soft mode along the [$\xi\xi$0] direction is of nearly perfect acoustic character, unlike the soft mode in the Fe-based magnetic shape memory (MSM) system Fe_3Pt, where the corresponding relaxation is driven by the Fe atoms

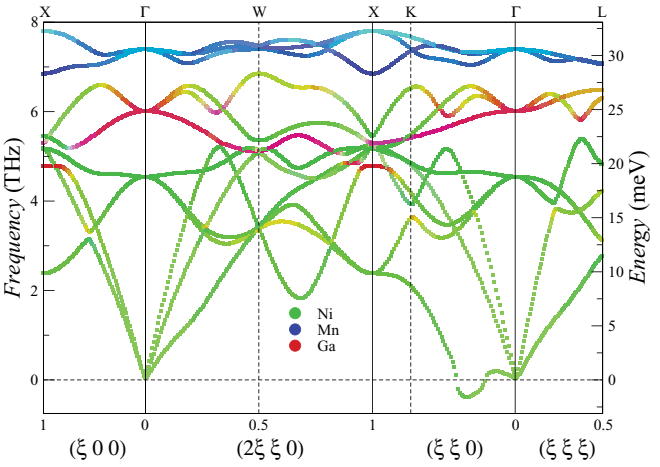

FIG. 2. (Color) The phonon dispersion calculations of the stoichiometric Ni_2MnGa sample for the high-symmetry directions of the $L2_1$ structure. The color coding represents the elemental contribution to the vibrational modes.

alone.[35] Another anomalous feature of the dispersion is the behavior of the optical modes which can be associated with the Ga atoms. According to the relative masses of the atoms, the frequencies of these modes should be lower than the frequencies of the modes that are related to oscillations of the Ni atoms. However, this normal-mode behavior is present only at the X point, while for all other regions of the Brillouin zone the branches associated with the Ni atoms are found to be the lowest-lying optical modes. In contrast to this, the optical modes that are related to the Mn atoms reveal a regular behavior and are found at the highest frequency values of the spectrum. At the same time, no hybridization of the Mn modes with other modes takes place, and a band gap between these modes and the rest of the spectrum is observed. The full phonon dispersion containing the elemental contribution is plotted in Fig. 2. The greenish color of the acoustic branches is related to the fact that the number of Ni atoms contributing to acoustic modes is twice as high as the number of the other atom types that contribute to the acoustic modes.

In a different approach and in order to parametrize the experimental phonon data a Born–von Kármán (BvK) force-constant model was fitted to the measured phonons. From that force constants up to the ninth nearest-neighbor shell have been extracted. The fitting was done by means of the GENAX program of Reichardt.[36] It enables us to compute the total and partial densities of states for the different atoms and to compare these to the results of the *ab initio* calculations.

V. RESULTS AND DISCUSSION

A. Phonon dispersion of stoichiometic Ni_2MnGa

The phonon dispersion of the Heusler $L2_1$ structure was measured for the high-symmetry directions along [ξ00], [$\xi\xi$0], and [$\xi\xi\xi$] and for the [2$\xi\xi$0] direction. Figure 3 shows the phonon dispersion of the stoichiometric composition Ni_2MnGa measured by inelastic neutron spectroscopy at room temperature. Solid and open symbols correspond to transverse and longitudinal polarizations, respectively. For the [ξ00] and [$\xi\xi\xi$] directions the transverse polarizations are degenerate,

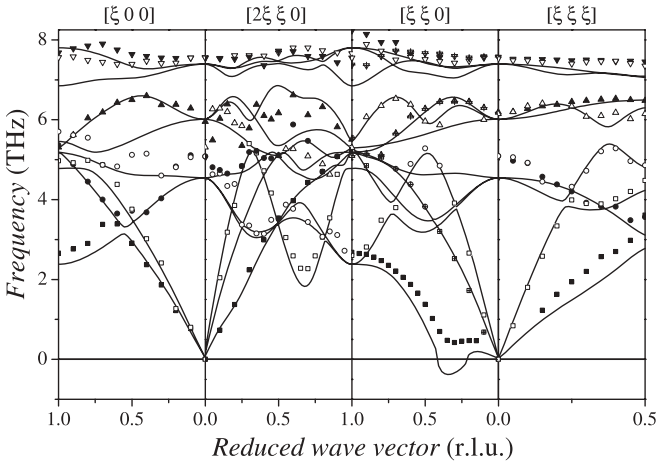

FIG. 3. The phonon dispersion of the stoichiometric Ni_2MnGa sample for the high-symmetry directions of the $L2_1$ structure. The symbols indicate the experimental results taken at room temperature. The lines represent the first-principles calculations from Fig. 2, here shown without color coding.

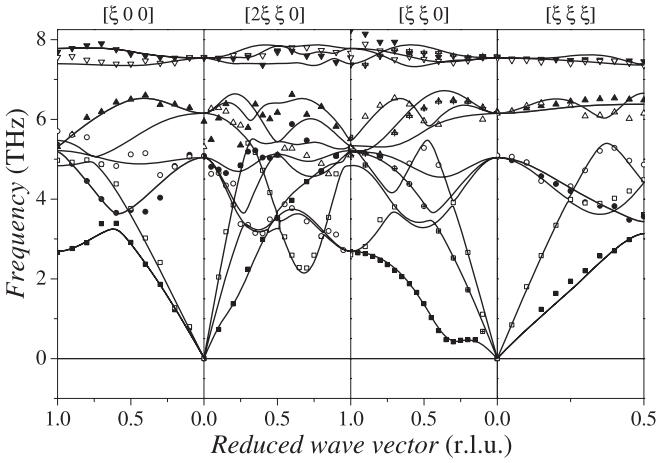

FIG. 4. Phonon dispersion of stoichiometric Ni_2MnGa. Symbols indicate the experimental results taken at room temperature (as in Fig. 3). Solid lines indicate the phonon dispersion obtained by fitting BvK force constants up to the ninth nearest-neighbor shell to the experimental results.

which is not the case for the $[\xi\xi 0]$ and $[2\xi\xi 0]$ directions. Different symbols represent different branch groups. Here squares show the acoustic modes, while circles, up triangles, and down triangles correspond to first, second, and third optical branches, respectively. Measurements of the slopes in the longitudinal $[\xi\xi 0]$ direction and the transverse $[\xi 00]$ branches as reported in the literature[14] agree well with our experimental study. The investigation of the acoustic phonons in Ref. 15 could be reproduced as well. The assignments of the branches to acoustic and optical modes, however, differ significantly. The solid lines are the computed phonon frequencies corresponding to 0 K obtained from our first-principles calculations, which agree well with previously derived results of Bungaro *et al.*[37] While the latter results were obtained using density functional perturbation theory, the results which are presented in our work have been obtained using the direct approach, where the force-constant matrices are calculated by displacing atoms within a sufficiently large supercell and computing the forces which appear due to this distortion. The same method has already been applied on Ni_2MnGa by Zayak *et al.* in the past; they concentrated on the phonon dispersion and vibrational DOS along the $[\xi\xi 0]$ direction.[38]

The calculations exhibit imaginary frequencies for the $TA_2[\xi\xi 0]$ phonon branch. This indicates the instability of the $L2_1$ structure at 0 K. The experimental results at room temperature confirm this instability in so far as the $TA_2[\xi\xi 0]$ phonon branch softens considerably, exactly at the point where these imaginary frequencies occur in the calculations. However, the measurements are taken at 300 K where the $L2_1$ phase is thermodynamically stable. The instability of the austenite phase towards lower temperatures shows up in a considerable softening of the phonon modes with decreasing temperature. The polarization and q values of these modes indicate the transition path for a reconstructive and diffusionless phase transition similar to what has been observed in high-temperature bcc phases of the d^1 and d^2 transition metals.[39–41] A further difference between calculations and measurements is obvious. Many of the calculated optical frequencies at the Γ point are lower than the measured ones.

In order to derive thermodynamical quantities harmonic force constants were fitted to the experimental phonon frequencies of Ni_2MnGa using the the BvK model. For each interaction a longitudinal and a transverse force constant were adjusted. The BvK fit taking into account interaction up to the ninth nearest-neighbor shell is shown in Fig. 4. Only such fits were retained where the square of the eigenvectors of the phonons corresponded to the measured and normalized intensities in the respective Brillouin zone. Due to the large number of fitting parameters, the dispersion relation according to the BvK model fits very well; in particular the softening in the $TA_2[\xi\xi 0]$ phonon branch is well described.

The total and partial vibrational DOS are calculated from the force constants obtained from the BvK model as well as from first-principles calculations, both shown in Fig. 5. Both vibrational DOS calculations perfectly reproduce the measured gap in the optical band around 7 THz—see Fig. 4. The partial DOS from first-principles calculations and the BvK model calculations resemble each other very much as well, but certainly the BvK fit represents better the measured dispersion. This analysis reveals that the high-frequency optical branch is mainly occupied by the lightest component (Mn) of the alloy. The low-frequency optical branch around 5 THz is mainly occupied by the Ni atoms, whereas the optical branch around 6 THz is occupied equally by Ni and Ga atoms.

The anomalous behavior found by Zayak *et al.* for phonon modes along the $[\xi\xi 0]$ direction,[38] namely, that the Ga atoms, which have the largest mass of all involved elements, do not have a dominant contribution to the low-frequency optical branches, is also present along other directions through the Brillouin zone, as was pointed out in the discussion of the *ab initio* phonon dispersion—see Fig. 2. The direct comparison of the vibrational DOSs shows that the Ni contribution to the low-lying optical frequencies, in particular the peak at about 4.65 THz, is even more pronounced when modes along

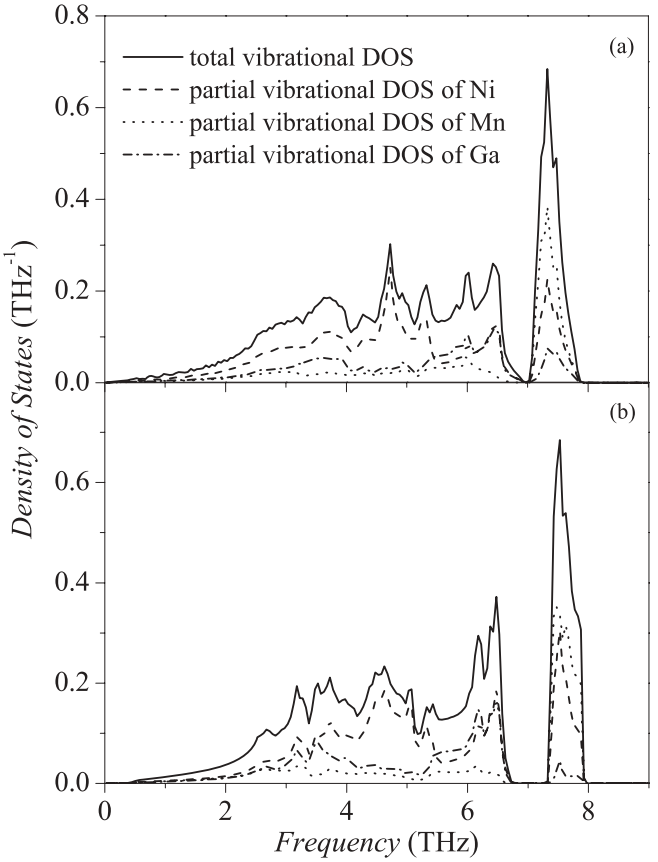

FIG. 5. Total and partial vibrational densities of states in Ni_2MnGa calculated from (a) first principles and (b) the BvK model.

the whole Brillouin zone are taken into account, compared to the results by Zayak *et al.*, who concentrated on the [$\xi\xi$0] direction only. The comparison with the experimental DOS demonstrates that the anomalous behavior of the optical modes is indeed present in the whole Brillouin zone, which confirms the previous analysis of Zayak *et al.*

The important softening observed in the TA_2[$\xi\xi$0] phonon branch does not show up as a pronounced feature in the DOS. This underlines the fact that this softening is particular for this propagation vector and is not extended along the four-dimensional dispersion surface. It can be regarded as a further indication that this softening plays the key role in the structural phase transition in relation to the transformation path.[41]

B. Phonon dispersion of off-stoichiometric $Ni_{49}Mn_{32}Ga_{19}$

Figure 6 shows the measured phonon dispersion of $Ni_{49}Mn_{32}Ga_{19}$ at 373 K. The phonon softening in the TA_2[$\xi\xi$0] phonon branch is shifted to smaller ξ values and is less pronounced compared to that in Ni_2MnGa. Similar softening properties of the TA_2[$\xi\xi$0] phonon branch have been reported in the literature for Ni-rich[16,17] and Mn-rich compositions[16] of Ni-Mn-Ga alloys. In the work of Mañosa *et al.*[16] for Ni-rich measurements the minimum of the softening is observed at $\xi = 0.33$ r.l.u., which corresponds to the premartensite transition. For the Mn-rich sample the softening minimum shifts to smaller value of ξ. In the study of Stuhr *et al.*[17] the vibrational properties of the Ni-rich sample were investigated.

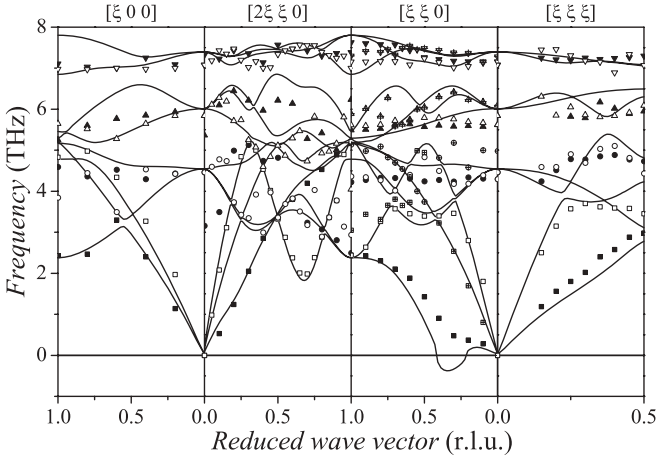

FIG. 6. The phonon dispersion of the $Ni_{49}Mn_{32}Ga_{19}$ sample in the austenite state. Lines indicate the first-principles calculations for the stoichiometic Ni_2MnGa at absolute zero temperature. The inelastic neutron scattering measurement were done at 373 K.

The result of that work shows that in the Ni-rich sample the minimum of the softening in the TA_2[$\xi\xi$0] phonon branch also shifts to smaller values of ξ. The comparison of these two investigations confirms that small changes in the chemical composition drastically change the vibrational properties.

The effect of compositional change is also visible on the optical branches. Compared to Ni_2MnGa all optical branches show less dispersion. Especially in the region around 6 THz the dispersion is determined by the dynamics of the Ga sites—see Fig. 2. There the reduced dispersion can be explained by an increased variation of the interaction coefficients caused by the off-stoichiometric composition.

C. Temperature-dependent phonon measurements

Typically for Ni-Mn-Ga alloys, small compositional variations cause considerable changes in the magnetic and structural transition temperatures.[9,10] The composition also affects the low-temperature structure of the corresponding alloys. On cooling stoichiometric Ni_2MnGa, the structure changes phase through the sequence $L2_1 \xrightarrow{270\ K} 3M$ (premartensite) $\xrightarrow{220\ K}$ NM (nonmodulated martensite[42]) phase. The corresponding sequence for $Ni_{49}Mn_{32}Ga_{19}$ is $L2_1 \xrightarrow{361\ K} 5M$ (five-layer modulated martensite).

We therefore performed a detailed study of the temperature dependence of the TA_2[$\xi\xi$0] phonon branch in Ni_2MnGa and $Ni_{49}Mn_{32}Ga_{19}$. Figure 7 shows temperature-dependent measurements in both compositions and the respective modulated phases. For both compositions, the anomalous softening is visible even for the highest temperatures well above the phase transition temperature.

Figure 7(a) clearly shows that the softening in Ni_2MnGa is restricted to a narrow range in the TA_2[$\xi\xi$0] phonon branch, ranging from approximately $\xi = 0.2$ to $\xi = 0.5$ r.l.u. The phonon frequencies for higher ξ values remain unchanged. This holds true even for the low-temperature measurement at 225 K in the modulated premartensitic 3*M* phase. For the stoichiometric Ni_2MnGa composition, the softening behavior of the TA_2[$\xi\xi$0] phonon branch as a function of temperature

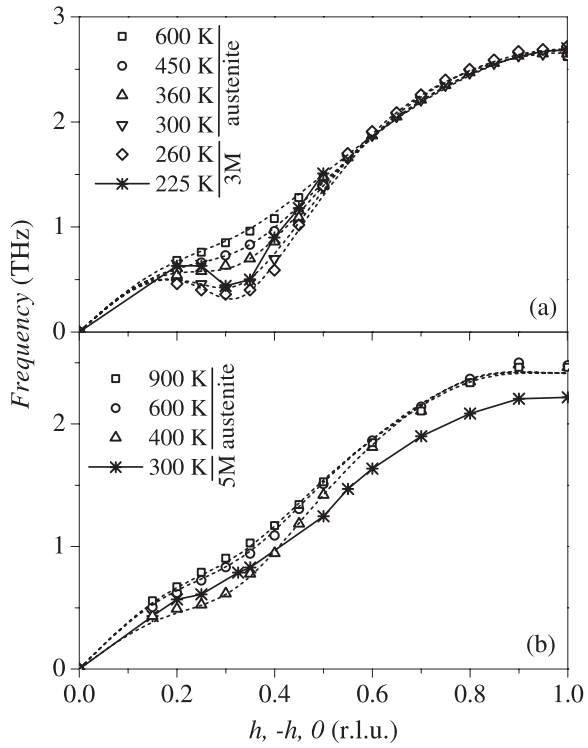

FIG. 7. The $TA_2[\xi\xi 0]$ phonon modes of (a) Ni_2MnGa and (b) $Ni_{49}Mn_{32}Ga_{19}$ for different temperatures. Dashed lines in (a) show BvK fits to the corresponding temperatures of the austenite phase. In (b) the dashed and solid lines are guides for the eye in the austenite phase and martensite phase, respectively.

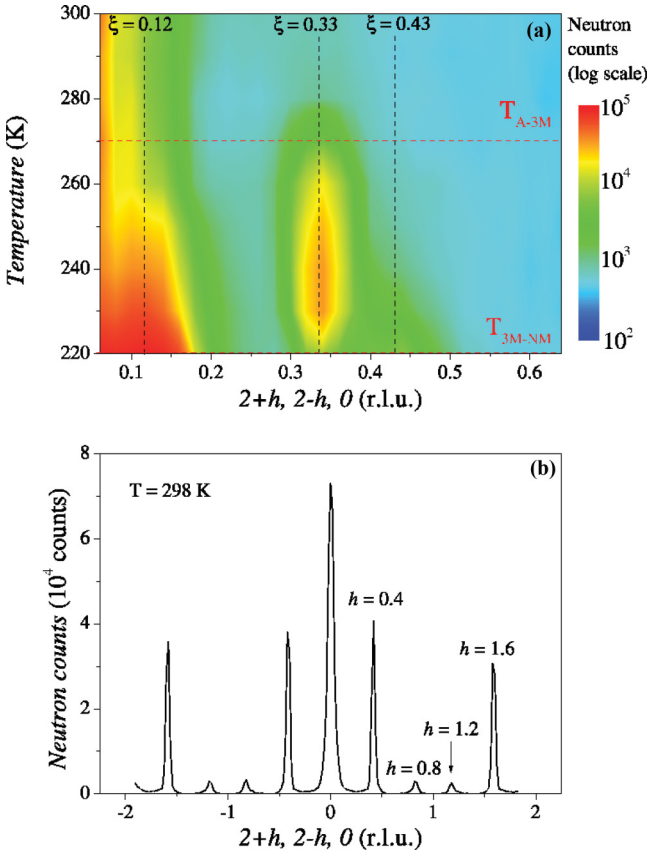

FIG. 8. (Color) (a) Intensity plot of the occurrence of the 3*M* phase on cooling stoichiometric Ni_2MnGa. The color code represents the neutron intensity in a logarithmic scale. (b) Elastic measurement of 5*M* martensite at 298 K. Superstructure Bragg peaks of the martensite phase show commensurate positions.

has been reported in the literature.[14,15] In the work of Zheludev *et al.*,[14] the observed phonon softening minimum at $\xi = 0.3$ r.l.u. for 260 K reaches down to 0.23 THz. In our study the observed minimum for the same condition is at 0.36 THz. The reason for this difference might be small changes in the composition and/or different resolution conditions in the experimental setups.

A slightly different picture shows up for the off-stoichiometric composition in Fig. 7(b). Here, the entire phonon branch is at lower frequencies. The softening itself is smeared out and less pronounced. Compared to the measurement in the austenitic phase, the martensitic 5*M* phase at 300 K is of even lower frequency along the entire phonon branch. The difference in the dynamic behavior of the two compositions is related to a difference in the nature of the phase transition concerning the changes to 3*M* and 5*M*, respectively. Whereas the transition to the 5*M* modulations shows up as a strong first-order transition with a clear signature in the DSC and magnetization measurements, the transition to the 3*M* phase is of sluggish nature—see Fig. 1.

References 43 and 44 also report no well-defined transformation energy of the transition to 3*M*. Following the structural Bragg peaks along the $[\xi\xi 0]$ direction as depicted in Fig. 8(a) an extended region in temperature with increasing and decreasing Bragg intensity is observed. As this does not correspond to a strong first-order transition, the 3*M* phase has been called premartensitic. The temperature dependence of the elastic intensity of the premartensite superstructure peak, $\xi = 0.33$ r.l.u., has been investigated in stoichiometric Ni_2MnGa by Zheludev *et al.*[14] The overall behaviors of the observed intensities of the present work and Ref. 14 fit quite well. We also confirm that after the premartensite transition, the stoichiometric alloy changes its structure to a nonmodulated tetragonal phase which shows a superstructure Bragg peak at $\xi = 0.43$ r.l.u. This superstructure Bragg peak of the nonmodulated tetragonal phase has been observed by Shapiro *et al.*[45] A similar increase of the intensity at $\xi = 0.12$ r.l.u. has been reported by Stuhr *et al.*[13] In our measurement this peak is shifted to $\xi = 0.17$ r.l.u. The interpretation of this rising intensity remains open. In Fig. 8(b) an elastic measurement of $Ni_{49}Mn_{32}Ga_{19}$ is shown for $T = 298$ K. The measurement is carried out around the 220 Bragg reflection of the martensite phase in both positive and negative transverse directions. In contrast to the stoichiometric composition, in $Ni_{49}Mn_{32}Ga_{19}$ the modulation is observed as superstructure Bragg peaks at repeated commensurate positions with the modulation vector of 0.4 r.l.u. This observation of the modulation vector agrees well with the existing powder x-ray diffraction literature.[46]

The question may arise whether the softening of the phonons stabilizes the austenite phase with respect to the martensite ground state. In the modified Landau expansion the square of the soft-mode frequency is interpreted as an order parameter driving the transition. The square of the frequency of the soft mode is expected to decrease linearly with

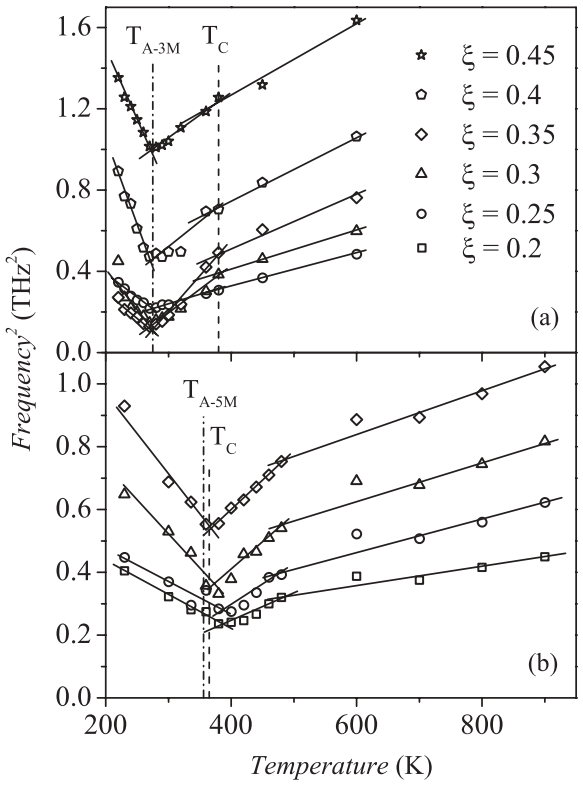

FIG. 9. Frequency squared as a function of temperature for different ξ values around the softening minimum of (a) the stoichiometric Ni_2MnGa alloy and (b) the off-stoichiometric $Ni_{49}Mn_{32}Ga_{19}$ alloy. $T_{A\text{-}3M}$ defines the premartensite transition temperature. Above this temperature the alloy has $L2_1$ Heusler structure and below this temperature the structure is three-layered modulated premartensite. T_{A-5M} defines the transition temperature from austenite to five-layered martensite of off-stoichiometric $Ni_{49}Mn_{32}Ga_{19}$. The solid lines are a guide to the eye. T_C represents the Curie temperatures for both stoichiometric and off-stoichiometric compositions.

temperature on approaching the phase transition temperature.[47–49] Figure 9 shows such plots for phonons at different ξ values around the minimum in the $TA_2[\xi\xi 0]$ phonon branch. The structural and magnetic transition temperatures as determined by our caloric and magnetization measurements are indicated for both samples. It is worth noting that these measurements were taken in the identical sample material as the phonon measurements. Extension of the temperature-dependent measurements to the modulated phases shows that the frequencies rise again. Whereas for the stoichiometric sample the transition to the 3*M* phase does not influence the structural integrity, the measurements in the off-stoichiometric 5*M* phase had to be done in another specially prepared sample. The similarity of the structures in the austenite and modulated martensite phases permitted us to study this phonon-mediated transition in detail. In both phases the structural transition is accompanied by the same phonon anomaly.

For the stoichiometric sample the slope in the plot of (Frequency^2) vs T changes distinctly around T_c. This coincidence has been interpreted as the onset of ferromagnetic ordering in the sample.[13,16,50] For the off-stoichiometric $Ni_{49}Mn_{32}Ga_{19}$ sample the structural and magnetic transition temperatures are close, 361 K for T_M and 371 K for T_c, respectively. The change in the slope of the phonon frequency squared versus temperature, however, remains similar to that in the stoichiometric sample, i.e., about 100 K above the structural transition. There is no obvious correlation of this dynamic anomaly with the magnetic ordering, which makes the interpretation for the stoichiometric sample questionable as well.

The modified Landau considerations help to relate the vibrational and structural behavior; however, they do not identify the causes for the structural changes. In analogy to the martensitic transformation to high-temperature bcc phases in the monatomic d^1 and d^2 elements, which predominantly stabilize via the vibrational entropy of soft modes,[39–41] it might be suggested that soft modes in the Ni_2MnGa system play a similar role. For instance, Enkovaara *et al.*[18] argue from first-principles calculations that the cubic to tetragonal transition in Ni_2MnGa is driven by the vibrational free energy. For clarifying such a hypothesis, the vibrational entropy of stoichiometric Ni_2MnGa has been calculated from the density of states $g(\nu)$, by using the well-known relation[51]

$$S_{\text{vib}} = -3k_B \int_0^\infty g(\nu)\{n(\nu)\ln[n(\nu)] - [1+n(\nu)]\ln[1+n(\nu)]\}d\nu, \quad (1)$$

where $n(\nu)$ is the Bose-Einstein distribution,

$$n(\nu) = \frac{1}{\exp\left(\frac{h\nu}{k_B T}\right) - 1}, \quad (2)$$

and h and k_B are Planck's constant and Boltzmann's constant, respectively. Three different approaches to $g(\nu)$ have been pursued. First, $g(\nu)$ resulting from the first-principles calculations has been used. The temperature dependence is then given by harmonic extrapolation from 0 K—see the solid line in Fig. 10. Second, the BvK fitted dispersion to the 300 K phonon measurements served to extract $g(\nu)$. The temperature-dependent vibrational entropy (S_{vib}) has been

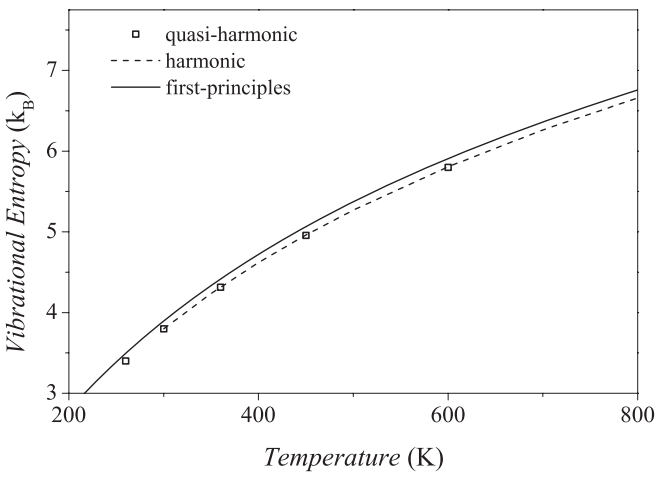

FIG. 10. Vibrational entropy calculations of Ni_2MnGa in the quasiharmonic (open dots) and in the harmonic (dashed line) approximations. The quasiharmonic approximation entropies are calculated from the DOS at the corresponding temperature. Harmonic entropies are extrapolated from the room-temperature DOS. The solid line depicts the first-principles calculations obtained using the harmonic approximation.

created by harmonic extrapolation from $S_{vib}(300\ K)$—see the dashed line in Fig. 10. Third, measurements of the phonon dispersion at different temperatures have been used to calculate $g(\nu)$ and subsequently S_{vib} at the given temperature. The last approach we call quasiharmonic, shown by open dots in Fig. 10. All approaches end up with minor differences with respect to $S_{vib}(T)$.

From the experimental observations we can state the following: Only the $TA_2[\xi\xi 0]$ phonon mode softens with decreasing temperature. This has been shown by measuring the temperature dependence of selected acoustic and optical branches. Therefore, unlike d^1 and d^2 refractory metals, for these materials only a very narrow region in **q** space shows a pronounced phonon softening, the weight of which does not suffice to influence $S_{vib}(T)$ strongly enough. Therefore the quasiharmonic S_{vib} does not deviate quantitatively from the harmonic S_{vib} at T_M. There is no hint that changes in S_{vib} stabilize the austenite phase. Figure 9 shows that the softenings of the phonons approach each other at the transition, coming from both temperature sides. Besides the structural change, the phonon frequencies are identical at the transition. As there is no jump in the phonon frequencies of these important branches, we conclude that there is no significant ΔS_{vib} at the transition temperature (Fig. 1).

Recent angular correlation of positron annihilation radiation (ARCAR) studies of the Fermi surface of stoichiometric Ni_2MnGa by Haynes *et al.*[52] combined with first-principles electronic structure calculations yield a further indication of the importance of magnetism for the phase stability of austenite. At 300 K, Fermi surface nesting is observed at $\xi = 0.47[110]$ r.l.u., a q vector which matches fairly well with the nonmodulated tetragonal martensite structure of the stoichiometric alloy at temperatures below 200 K. Furthermore, Haynes *et al.*[52] have simulated the influence of temperature by adjusting the total magnetic moment at the given temperature (Stoner approach). As a result the nesting vector shifts its position with temperature, matching $\xi = 0.43[110]$ r.l.u. at temperatures around the martensite transition temperature. This explanation of the phonon softening by Fermi surface nesting or electron-phonon interaction goes in hand with earlier first-principles calculations[53] and phonon measurements.[14,15,48]

VI. SUMMARY AND CONCLUSIONS

In this work we investigated the complete phonon dispersion and the effect of compositional changes on the vibrational properties of Ni-Mn-Ga samples by using the compositions Ni_2MnGa and $Ni_{49}Mn_{32}Ga_{19}$. Common to both compositions is a pronounced softening in the $TA_2[\xi\xi 0]$ phonon branch. *Ab initio* calculations exhibit imaginary frequencies at the position of these soft phonons in reciprocal space, thereby indicating the instability of the austenite phase. The position in q space reveals the transition path from austenite to tetragonal modulated martensite. Similarly to what has been observed for the martensitic transition in the d^1 and d^2 transition metals, this happens by shuffling (110) planes in the $[1\bar{1}0]$ direction.

The compositional change influences the vibrational properties of the material effectively. Whereas the optical phonon frequencies for the stoichiometric and off-stoichiometric samples are in about the same frequency band, the wave vector dependence, i.e., the dispersion character, is much more pronounced in the strongly ordered sample. For $Ni_{49}Mn_{32}Ga_{19}$, 20.7% of the excess Mn atoms are on regular Ga sites. So the interaction between different atomic sites varies and thereby the optical dispersion is smoothed.

The phonon softening in Ni_2MnGa has its minimum at $\xi = 0.33$ r.l.u., which corresponds to the commensurate position of the $3M$ phase. It is more pronounced when compared to $Ni_{49}Mn_{32}Ga_{19}$ which has the minimum at $\xi = 0.30$ r.l.u. The compositional disorder in this sample leads to a smearing of the phonon anomaly in **q** space. The phonon minimum shifts towards the commensurate position of the low-temperature $5M$ structure at $\xi = 0.28$ r.l.u.

The temperature dependence of the $TA_2[\xi\xi 0]$ phonon branch shows the same overall behavior for both samples. The square of the phonon frequency becomes soft without reaching zero frequency, while approaching the structural transition temperature from both sides. This has been described in a generalized Landau expansion. In the stoichiometric sample this temperature dependence of the softening of the $TA_2[\xi\xi 0]$ phonon coincides perfectly with the magnetic and structural transitions. In this way the Landau expansion reflects both the structural and magnetic ordering phenomena. This is not the case for the off-stoichiometric sample. In the case of the off-stoichiometric composition the temperature behavior of the phonon softening reflects the structural transition, but no obvious influence of the magnetic transition on the phonon softening is observed. To understand this different behavior a theoretical model of the interactions between magnetic ordering and lattice dynamics is required.[48] Here the relation between the magnetic ordering and the vibrational properties is still an open question.

Unlike the case of d^1 and d^2 transition metals, here the vibrational entropy originating from the softening of lattice vibrations alone is not enough to stabilize the austenite phase of Ni_2MnGa. For the transformation to the modulated phases, Fermi surface nesting can be seen as the driving force as predicted by first-principles calculations[19,54] and experimentally evidenced by positron annihilation measurements.[52]

ACKNOWLEDGMENTS

This work has been financially supported by the DFG Priority Program (SPP1239). We thank K. Rolfs and R. Schneider for producing the single crystals. Experimental help by T. Mehaddene and B. Pedersen at RESI, providing help for using the GENAX program by D. Lamago, is acknowledged.

*semih.ener@tum.de

†Also at Forschungs-Neutronenquelle Heinz Maier-Leibnitz (FRM II), Technische Universität München, D-85747 Garching, Germany.

‡Also at Institut für Physikalische Chemie, Georg-August Universität, D-37077 Göttingen, Germany.

[1] *Shape Memory Effect*, edited by H. Funakubu (Gordon and Breach Science Publishers, New York, 1987).

[2]P. J. Webster, K. R. A. Ziebeck, S. L. Town, and M. S. Peak, Philos. Mag. B **49**, 295 (1984).
[3]A. Gonzàlez-Comas, E. Obradó, L. Mañosa, A. Planes, V. A. Chernenko, B. J. Hattink, and A. Labarta, Phys. Rev. B **60**, 7085 (1999).
[4]W. H. Wang, J. L. Chen, S. X. Gao, G. H. Wu, Z. Wang, Y. F. Zheng, L. C. Zhao, and W. S. Zhan, J. Phys.: Condens. Matter **13**, 2607 (2001).
[5]F. Zuo, X. Su, and K. H. Wu, Phys. Rev. B **58**, 11127 (1998).
[6]V. V. Khovailo, T. Takagi, A. D. Bozhko, M. Matsumoto, J. Tani, and V. G. Shavrov, J. Phys.: Condens. Matter **13**, 9655 (2001).
[7]V. A. Chernenko, J. Pons, C. Seguí, and E. Cesari, Acta Mater. **50**, 53 (2002).
[8]A. N. Vasil'ev, A. D. Bozhko, V. V. Khovailo, I. E. Dikshtein, V. G. Shavrov, V. D. Buchelnikov, M. Matsumoto, S. Suzuki, T. Takagi, and J. Tani, Phys. Rev. B **59**, 1113 (1999).
[9]A. Planes, L. Mañosa, and M. Acet, J. Phys.: Condens. Matter **21**, 233201 (2009).
[10]P. Entel, V. D. Buchelnikov, V. V. Khovailo, A. T. Zayak, W. A. Adeagbo, M. E. Gruner, H. C. Herper, and E. F. Wassermann, J. Phys. D **39**, 865 (2006).
[11]A. Sozinov, A. A. Likhachev, N. Lanska, and K. Ullakko, Appl. Phys. Lett. **80**, 1746 (2002).
[12]S. J. Murray, M. Marioni, S. M. Allen, R. C. O'Handley, and T. A. Lograsso, Appl. Phys. Lett. **77**, 886 (2000).
[13]U. Stuhr, P. Vorderwisch, V. V. Kokorin, and P.-A. Lindgård, Phys. Rev. B **56**, 14360 (1997).
[14]A. Zheludev, S. M. Shapiro, P. Wochner, A. Schwartz, M. Wall, and L. E. Tanner, Phys. Rev. B **51**, 11310 (1995).
[15]A. Zheludev, S. M. Shapiro, P. Wochner, and L. E. Tanner, Phys. Rev. B **54**, 15045 (1996).
[16]L. Mañosa, A. Planes, J. Zarestky, T. Lograsso, D. L. Schlagel, and C. Stassis, Phys. Rev. B **64**, 024305 (2001).
[17]U. Stuhr, P. Vorderwisch, and V. V. Kokorin, J. Phys.: Condens. Matter **12**, 7541 (2000).
[18]J. Enkovaara, A. Ayuela, L. Nordstrom, and R. M. Nieminen, J. Appl. Phys. **91**, 7798 (2002).
[19]M. A. Uijttewaal, T. Hickel, J. Neugebauer, M. E. Gruner, and P. Entel, Phys. Rev. Lett. **102**, 035702 (2009).
[20]M. Siewert, M. E. Gruner, A. Dannenberg, A. Chakrabarti, H. C. Herper, M. Wuttig, S. R. Barman, S. Singh, A. Al-Zubi, T. Hickel, J. Neugebauer, M. Gillessen, R. Dronskowski, and P. Entel, Appl. Phys. Lett. **99**, 191904 (2011).
[21]K. Rolfs, M. Chmielus, J. M. Guldbakke, R. C. Wimpory, A. Raatz, W. Petry, P. Müllner, and R. Schneider, Adv. Eng. Mater. **14**, 614 (2012).
[22]B. Pedersen, S. Ener, and J. Neuhaus (unpublished).
[23]P. Entel, V. D. Buchelnikov, M. E. Gruner, A. Hucht, V. V. Khovailo, S. K. Nayak, and A. T. Zayak, Mater. Sci. Forum **583**, 21 (2008).
[24]S. Aksoy, M. Acet, P. P. Deen, L. Mañosa, and A. Planes, Phys. Rev. B **79**, 212401 (2009).
[25]V. D. Buchelnikov, P. Entel, S. V. Taskaev, V. V. Sokolovsky, A. Hucht, M. Ogura, H. Akai, M. E. Gruner, and S. K. Nayak, Phys. Rev. B **78**, 184427 (2008).
[26]G. Kresse, J. Furthmüller, and J. Hafner, Europhys. Lett. **32**, 729 (1995).
[27]X. Gonze and C. Lee, Phys. Rev. B **55**, 10355 (1997).
[28]K. Parlinski, Z.-Q. Li, and Y. Kawazoe, Phys. Rev. Lett. **78**, 4063 (1997).
[29]G. Kresse and J. Furthmüller, Phys. Rev. B **54**, 11169 (1996).
[30]G. Kresse and D. Joubert, Phys. Rev. B **59**, 1758 (1999).
[31]P. E. Blöchl, Phys. Rev. B **50**, 17953 (1994).
[32]J. P. Perdew, K. Burke, and M. Ernzerhof, Phys. Rev. Lett. **77**, 3865 (1996).
[33]M. Methfessel and A. T. Paxton, Phys. Rev. B **40**, 3616 (1989).
[34]D. Alfé, Comput. Phys. Commun. **180**, 2622 (2009).
[35]M. E. Gruner, W. A. Adeagbo, A. T. Zayak, A. Hucht, and P. Entel, Phys. Rev. B **81**, 064109 (2010).
[36]W. Reichardt (private communication).
[37]C. Bungaro, K. M. Rabe, and A. Dal Corso, Phys. Rev. B **68**, 134104 (2003).
[38]A. T. Zayak, P. Entel, K. M. Rabe, W. A. Adeagbo, and M. Acet, Phys. Rev. B **72**, 054113 (2005).
[39]W. Petry, A. Heiming, J. Trampenau, M. Alba, C. Herzig, H. R. Schober, and G. Vogl, Phys. Rev. B **43**, 10933 (1991).
[40]A. Heiming, W. Petry, J. Trampenau, M. Alba, C. Herzig, H. R. Schober, and G. Vogl, Phys. Rev. B **43**, 10948 (1991).
[41]W. Petry, in *Proceedings of the Third European Symposium on Martensitic Transformations (ESOMAT 94)*, edited by A. Planes, J. Ortín, and L. Manosa (EDP Sciences, Les Ulis (France), 1994) [J. Phys. IV **5**, 15 (1995)].
[42]In the literature the $\xi = 0.43$ r.l.u. peak is also considered as an incommensurate modulated tetragonal phase peak.
[43]S. Banik, A. Chakrabarti, U. Kumar, P. K. Mukhopadhyay, A. M. Awasthi, R. Ranjan, J. Schneider, B. L. Ahuja, and S. R. Barman, Phys. Rev. B **74**, 085110 (2006).
[44]F. J. Pérez-Reche, E. Vives, L. Mañosa, and A. Planes, Mater. Sci. Eng. A **378**, 353 (2004).
[45]S. M. Shapiro, P. Vorderwisch, K. Habicht, K. Hradil, and H. Schneider, Europhys. Lett. **77**, 56004 (2007).
[46]L. Righi, F. Albertini, L. Pareti, A. Paoluzi, and G. Calestani, Acta Mater. **55**, 5237 (2007).
[47]J. A. Krumhansl and R. J. Gooding, Phys. Rev. B **39**, 3047 (1989).
[48]A. Planes, E. Obradó, A. Gonzàlez-Comas, and L. Mañosa, Phys. Rev. Lett. **79**, 3926 (1997).
[49]S. M. Shapiro, in *Magnetism and Structure in Functional Materials*, edited by A. Planes, L. Mañosa, and A. Saxena, Vol. 6 (Springer, Berlin, 2006), Chap. 6, pp. 93–112.
[50]T. Castán, A. Planes, and A. Saxena, Phys. Rev. B **67**, 134113 (2003).
[51]H. Schober and W. Petry, Mater. Sci. Technol. **1**, 289 (1993).
[52]T. D. Haynes, R. J. Watts, J. Laverock, Z. Major, M. A. Alam, J. W. Taylor, J. A. Duffy, and S. B. Dugdale, New J. Phys. **14**, 035020 (2012).
[53]Y. Lee, J. Y. Rhee, and B. N. Harmon, Phys. Rev. B **66**, 054424 (2002).
[54]M. E. Gruner, W. A. Adeagbo, A. T. Zayak, A. Hucht, S. Buschmann, and P. Entel, Eur. Phys. J. Spec. Top. **158**, 193 (2008).